Magnetic Resonance Imaging 33 (2015) 328–335

Contents lists available at ScienceDirect

Magnetic Resonance Imaging

journal homepage: www.mrijournal.com

Desktop MRI as a promising tool for mapping intra-aneurismal flow

Josefina Perlo [a], Emilia V. Silletta [b], Ernesto Danieli [a,*], Giorgio Cattaneo [c], Rodolfo H. Acosta [b], Bernhard Blümich [a], Federico Casanova [d]

[a] Institut für Technische und Makromolekulare Chemie, RWTH Aachen University, Worringerweg 1, 52062 Aachen, Germany
[b] FaMAF-Universidad Nacional de Córdoba & IFEG-CONICET, Córdoba, Argentina
[c] Acandis GmbH u. Co. KG, Theodor-Fahrner-Strasse 6, 75177 Pforzheim, Germany
[d] Magritek GmbH, Philipsstrasse 8, 52068 Aachen, Germany

ARTICLE INFO

Article history:
Received 22 August 2014
Revised 17 November 2014
Accepted 8 December 2014

Keywords:
Compact MRI
Aneurysm
Flow
Metallic stent
Flow diverter

ABSTRACT

In this work we evaluate the performance of a 40-mm diameter bore 0.2 T desktop Halbach tomograph to obtain 2D and 3D velocity maps for studying intra-aneurismal flow in the presence or absence of nitinol meshed implants with the aim of optimizing the flow diverter efficacy. Phantoms with known spatial velocity distribution were used to determine the performance of the MRI system. Maximum velocities of about 200 mm/s could be measured with a precision of 1% at a spatial resolution of $0.5 \times 0.5 \times 1$ mm^3. This accuracy is suitable to evaluate *in vitro* intra-aneurismal flow under different conditions such as variable flow rates, different vessel-aneurysm geometry, as well as the influence of metallic flow diverters on the intra-aneurismal flow distribution. The information obtained non-invasively with desktop tomographs can be used to complement *in vivo* studies in order to decide the optimum flow diverter.

1. Introduction

Aneurysms are localized bulgy malformations in the walls of blood vessels. Their growth and rupture strongly depend on the blood flow distribution inside the cavity [1] and can have a significant adverse impact on the life of the patient [2]. Minimally invasive therapy targets at the intra-aneurismal blood clotting by reducing or stopping intra-aneurismal blood flow as a means to initiate vessel regeneration. In general, this is achieved by inserting endovascular coils with the help of micro catheters. However, due to positioning instabilities in wide neck aneurysm, thromboembolism, and intra-procedural aneurysm perforation [3], a different approach based on the use of stent-like "flow diverters" (FDs) has recently been suggested [4]. This new generation of implants used to induce blood exclusion or deceleration within the aneurysm is fabricated as a tubular mesh structure with a defined porosity that is inserted into the vessel to reduce the blood flow directed into the aneurysm and generate long-term blood clotting to minimize risk of rupture.

The influence of FDs on the flow distribution inside the aneurysm, and its further implications on intra-aneurismal clot formation is not yet completely understood. The interplay of different physiological parameters such as aneurysm geometry, location, size, hemodynamic variables (blood velocity, pressure, residence time), and flow-diverter specifications such as porosity or cell size of the device, influence the degree and the time of the aneurysm occlusion. Recent *in vivo* studies have reported that the porosity of FDs can change with subsequent alterations in their performance [5]. It has also been shown that aneurysm rupture can occur in patients after treatment with an FD as a consequence of flow-driven, uncontrolled clot formation resulting in thrombus-associated autolysis [6], or mural destabilization of the aneurysm wall due to thrombus evolution [7]. This suggests that for each patient, FD parameters need to be varied until the flow diversion that leads to optimal clot formation speed is achieved. Such a task is very time-consuming and cannot be carried out *in vivo*, because it would require an iterative procedure involving the insertion of an FD in the patient vessel, a subsequent measurement of the effect of such FD on the intra-aneurismal flow, and an evaluation of the results. Then, the procedure would have to start again with a different FD. Instead, the common practice is to perform 3D angiography of the aneurysm zone of each patient. Once the information about the shape, size and location of the aneurysm has been obtained by 3D angiography, the influence of different FDs on the flow distribution can be determined by using computational fluid dynamics (CFD) [8,9]. Another approach is to produce a phantom of the aneurysm and to study the problem limited to *in vitro* examinations with different experimental techniques. Then, the results obtained by correlating the changes in the intra-aneurismal flow distribution introduced by positioning FDs of different characteristics inside the phantom could be used to select the optimum device specifications suitable for each particular case.

* Corresponding author at: ITMC-RWTH-Aachen University, Worringerweg 1, 52074 Aachen, Germany Room 38B/011B. Tel.: +49 241 8026794.
E-mail address: danieli@itmc.rwth-aachen.de (E. Danieli).

http://dx.doi.org/10.1016/j.mri.2014.12.005
0730-725X/

Model phantoms have been employed for describing flow in the aortic arc [10], to evaluate flow in the presence of in-stent stenosis [11,12], and to monitor the flow reduction induced by different stent porosities in intra-aneurismal flow [1,13–15]. Techniques such as particle image velocimetry (PIV) [1,16], laser Doppler anemometry (LDA) [13,17], magnetic resonance imaging (MRI) [11] and ultrasound [18] can be used, depending on the characteristics of the phantom, to map the flow distributions. The fact that MRI does not require the use of tracking particles or contrast agents, that may alter the flow patterns, and that it is suitable for optically non-transparent media like blood, represents an advantage over the other optical methods. Additionally, it is sensitive to parameters associated with molecular mobility or density — information not always accessible with other techniques. Concerning clinical applications, MRI is a standard method which has attracted increasing interest for neurovascular diagnostics, because it is completely non-invasive. However, common practice of MRI involves the use of expensive magnets generating strong homogeneous magnetic fields that are not always available for time-consuming *in vitro* research.

In this work, we propose the use of a compact MRI tomograph built from permanent magnets to measure the velocity distributions inside vessel models for different geometries. We show that the performance of the MR tomograph prototype operating at a field strength of 0.2 T [19] is suitable to assess intra-aneurismal flow in the presence nitinol meshed implants. As a proof of principle, we compare the flow maps with and without an FD for different aneurysm models made of glass and silicone.

2. Methods

The experiments reported in this work were performed with a Halbach magnet built from identical permanent magnet blocks generating a magnetic field of 0.2 T, which corresponds to a resonance frequency of about 9 MHz for hydrogen nuclei [19]. Excitation and detection of the NMR signal was performed with a six-turn solenoid radiofrequency (rf) coil, 42 mm in diameter and 70 mm long. It was made from a copper sheet with a variable width calculated to maximize the homogeneity of the rf field. The magnet was equipped with a three-axis gradient coil system whose dimensions are 68 mm in diameter and 200 mm long. The efficiency of the transverse coils generating the gradients along x- and y-axes is 0.025 Tm^{-1} A^{-1}. The coil generating the field gradient along z (axis of the cylinder) has an efficiency of 0.013 Tm^{-1} A^{-1}. The coils can be switched on and off within ramp times of about 50 μs. The maximum achievable gradient strength is 0.5 Tm^{-1} along the x- and y-axes and 0.26 Tm^{-1} along the z-axis. They were driven by two double channel Techron LVC 5050 gradient amplifiers supplying a maximum output of 20 A per channel. A Magritek Kea2 spectrometer operating at a frequency of 9 MHz for ^{1}H was used for all experiments.

Among the different methods to encode velocity in NMR, the one most widely used is the application of a bipolar gradient pulse that inscribes a phase difference on the signal which is proportional to the velocity of the spin-bearing molecules. For a pair of gradient pulses of intensity G_{vel}, duration δ, and separation time Δ, the phase shift induced for a spin travelling at velocity v is $\Delta\varphi = \gamma\delta\Delta G_{vel}\, v$ [20,21]. The term γ is the gyromagnetic ratio of hydrogen nuclei. Velocity mapping by MRI relies on the application of velocity-encoding gradients which are included in the imaging sequence and have to be applied at any time prior to the frequency-encoding gradient and data acquisition (Fig. 1). The Hahn-echo sequence was used to image velocity distributions in order to reduce spurious effects due to magnetic field inhomogeneity. The map of the velocity along a given direction is obtained by calculating the phase difference between a reference image measured without velocity gradients and a second image measured with the bipolar gradient pulse applied along the desired spatial direction. A subtraction of the respective phases on a pixel-by-pixel basis allows the quantification of velocities. A 3D velocity vector map can then be derived from the 3D velocity component maps.

For all the experiments reported in this work, a glycerin/water mixture (mass ratio 43/57) with a viscosity of 3.6 cP at room temperature, that is comparable to that of blood, was used. The mixture was doped with $CuSO_4$ to reduce the relaxation time T_1 to approximately 160 ms. The flow rate through the system was driven by a Verder gear pump VG-1000 with a maximal flow rate of 80 ml/s arranged in a closed loop. For the present study, flow rates ranging from 0.1 ml/s to 2.0 ml/s were used, applicable to a range of Reynolds numbers from 0 to 400. A reservoir of the glycerin/water mixture was placed between the pump and the magnet to ensure a steady flow in the system. A pre-polarization volume of about 10 ml was placed inside the magnet before the rf coil region to ensure that spins in the solution spend approximately $5 \times T_1$ at the working field strength before entering the sensitive volume. Velocity images were acquired using a 3D spin-echo pulse sequence as shown in Fig. 1. A slice of 50 mm thickness along the z direction was used in all experiments. Along the read-direction 64 complex points were acquired with a dwell time of 10 μs. The **k**-space was sampled in phase directions with gradients varying from $-G_{max}$ to G_{max}. The typical nominal spatial resolution was in the range from 0.5 mm to 1 mm. The velocity-encoding gradients were applied before the 180°-refocusing pulse in the three spacial directions. All gradient pulses were generated using a 200 μs-duration ramp. There were 100 steps in the ramp between the initial and the final amplitude values, whereby a different gradient value was taken at every 2 μs. The other MR settings were: 90° Gaussian pulse length of 60 μs, 180° hard pulse length of 35 μs, echo time $t_E = 10$ ms, $\Delta = 1.802$ ms, $\delta = 1.4$ ms, and repetition time $t_R = 500$ ms. The images were stored and processed using Prospa V3 software in order to obtain the velocity maps. The computed intensity values represent the velocity in millimeters per second through each pixel.

A flow diverter with a diameter of 4.5 mm made from 48 braided nitinol wires of 40 μm diameter forming an angle of 75° was used (Fig. 2a). It is a development prototype provided by Acandis. For this investigation, the FD had open ends on both sides. Two aneurysm phantoms made of borosilicate glass were used. One of the phantoms represents a lateral aneurysm in a straight vessel (Fig. 2b) and the other one a lateral aneurysm in a V-shaped vessel (Fig. 2c). In both cases, the aneurysm is a sphere with a 10 mm inner diameter, and the vessel is a glass tube of 4 mm internal diameter. Finally, a silicone clone of a real ill-vessel consisting in a saccular aneurysm located in a tortous vessel segment (Fig. 2d) was used.

A test-sample consisting of two concentric cylindrical glass tubes aligned along the magnet axis (z-direction) with outer diameters of 13 mm and 4 mm and each having a wall thickness of 0.5 mm, was used to evaluate the performance of the 0.2 T Halbach tomograph to measure velocity. Both tubes were filled with the glycerin/water mixture. To set flow conditions, the fluid was pumped either through the inner tube or through the interstices between both tubes, thereby imposing a laminar regime in each case. 2D-velocity maps along the three axes were computed for a flow rate of 0.6 ml/s imposed through the inner tube. In order to determine the error of the velocity measurement, each velocity map was measured ten times.

The presence of metallic FD in the neighborhood of the sample can distort the MRI measurements due to B_0 distortions, rf shielding or induction of eddy currents. This distortion has been observed at typical clinical magnetic field strengths of 1.5 T and 3 T [22,23]. Thus, it is desirable to ensure that both the amplitude and the phase of the MR signal measured at a lower field strength of 0.2 T are accurate and independent of the presence of the metallic FD. Consequently, the nitinol FD (Fig. 2a) was placed on the exterior of the inner tube in

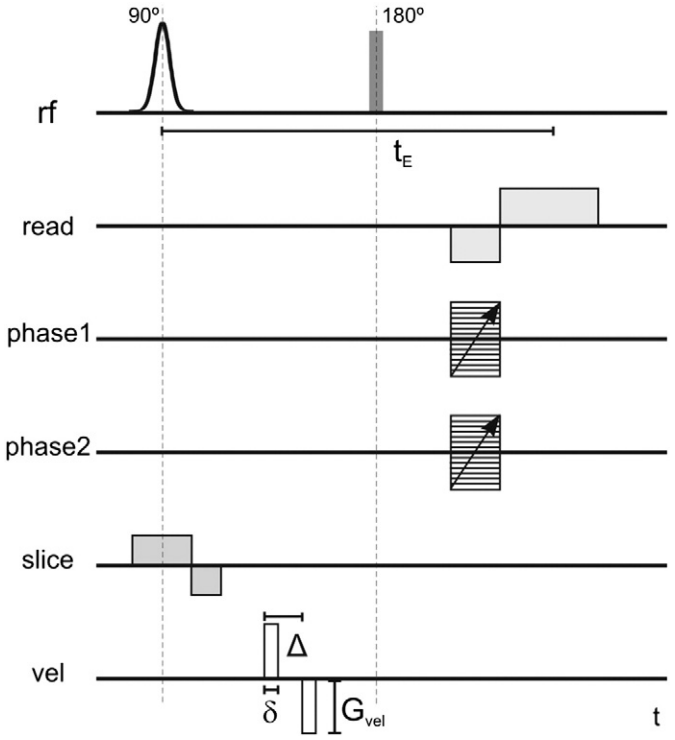

Fig. 1. 3D spin-echo pulse sequence with a bipolar gradient pulse to encode velocity. The experimental NMR parameters used for all the experiments were the following: 90° Gaussian rf pulse with 60 μs length, excitation slice of 50 mm thickness along the z axis, a rectangular 180° pulse with 35 μs length, 10 ms echo time (t_E), $\delta = 1.4$ ms, $\Delta = 1.802$ ms and a recycled delay of 500 ms.

the test-sample. To evaluate effects of the FD presence on the MR image, 3D images with and without the FD were acquired in non-flowing condition. Subsequently, in a first experiment, the flow sensitivity was tested by pumping the glycerin/water mixture in the laminar regime through the inner tube, and, in a second independent experiment, through the outer section. 3D maps of the z-velocity were acquired for flow along the z-axis with and without the FD.

To determine the influence of the vessel geometry on the intra-aneurismal flow, two glass phantoms were used in which each had a different vessel shapes (straight and V-shaped, Fig. 2b–c) where the velocity patterns under steady flow conditions are already known were used [1]. These geometries were chosen, because under steady flow conditions, the presence of vortices in the aneurysm strongly depends on the geometry of the vessel [1]. The geometry effects were evaluated by measuring 3D-velocity maps along the x- and z-axes under a 1.5 ml/s flow rate for both glass phantoms. The FD was inserted in the V-shaped vessel, and 3D intra-aneurismal velocity maps along x- and z-axes were computed for a 2.3 ml/s flow rate, with and without the FD. In order to assess the performance of the low-field tomograph in a more realistic scenario, a silicone clone of an ill-vessel mapped from a patient was used. Three-dimensional velocity maps along the three axes were computed with and without the FD.

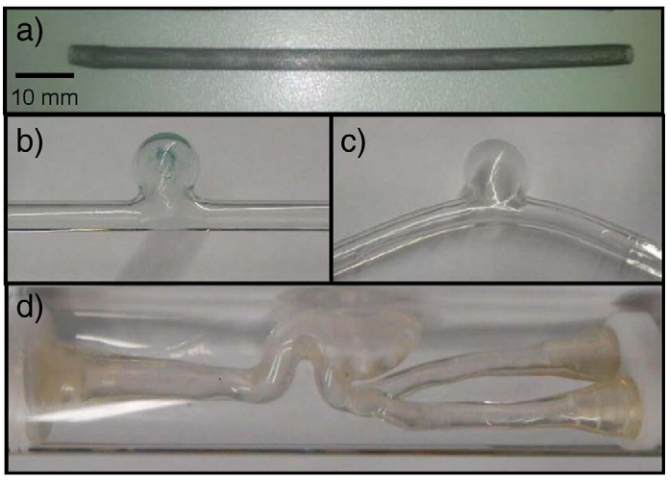

Fig. 2. Samples: a) Flow diverter. b) and c) Glass model of lateral aneurysm placed on a straight vessel and a V-shaped vessel, respectively. d) Aneurysm silicon clone.

3. Results

3.1. Flow measurements

The test-sample was used to evaluate the performance of the experimental setup. A signal phase variation of less than 0.5% was observed due to pump instabilities, which did not generate phase-encoding artifacts. The velocity maps in the test-sample under flow conditions through the inner tube showed the expected behavior (Fig. 3 a,b,c). The three velocity components fluctuated around the zero value in the outer tube as well as the x and y velocities in the inner tube; a parabolic velocity distribution was observed along the z-axis in the inner tube. The ten 1D profiles of the three velocity components generated inside the inner tube along the read (Fig. 3d) and phase directions (Fig. 3e) exhibited the same standard deviation which is about 0.05 radians of a maximum dephase of 2π. The error analysis was conducted on the velocity-encoded phases, which are obtained from the subtraction of the phases of two experiments: the first without and the second with applied velocity gradients. For a field of flow (FoF) of 200 mm/s that corresponds to 2π radians, the

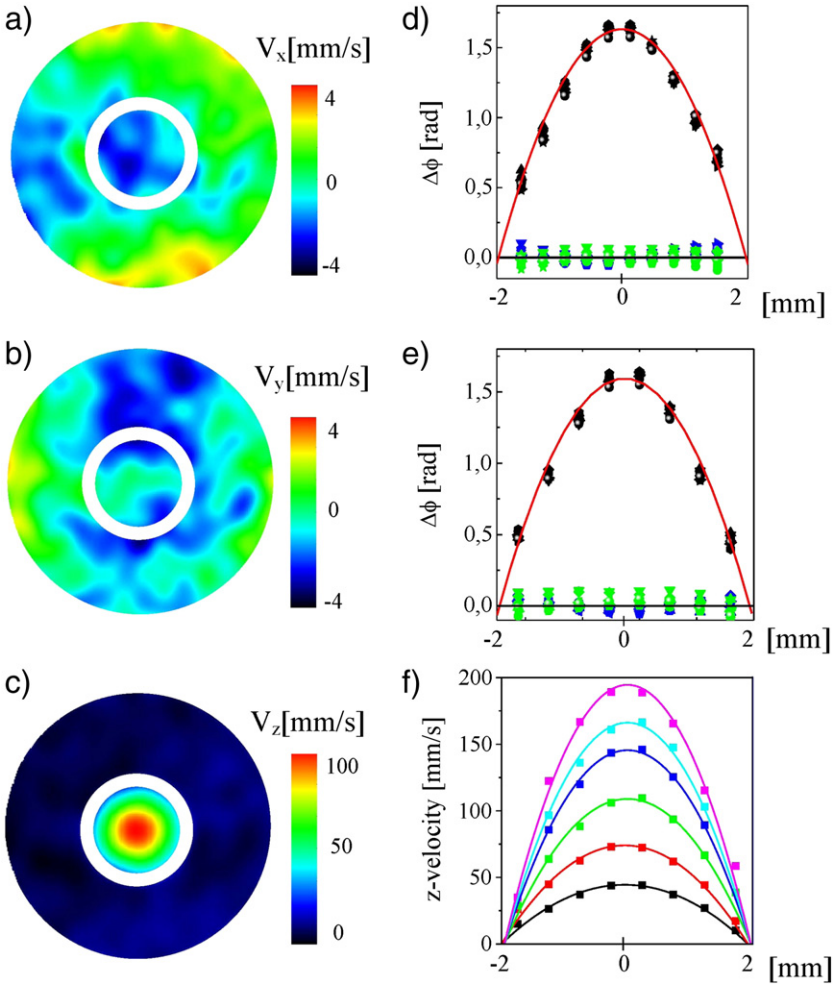

Fig. 3. Performance of the 0.2 T desktop MRI to measure velocity: a), b) and c) Velocity map of the component along the *x*-, *y*-, and *z*-axes, respectively for the test sample under laminar flow conditions through the inner tube and non-flowing conditions through the outer one for a flow rate of 0.6 ml/s. d) One dimensional *x*- (green), *y*- (blue) and *z*- (black) velocity distributions (ten independent experiments) inside the inner tube along the *x*-axis and e) along the *y*-axis. f) One-dimensional *z*-velocity distribution in the inner tube for different flow rates.

obtained error is 1.5 mm/s. Moreover, maps of the *z*-velocity component were measured for different flow rates inside the inner tube. Fig. 3f shows the corresponding 1D profile along the read direction. All of them present a parabolic velocity distribution and a linear correlation with the flow rate applied.

3.2. Artifacts

For density testing, the images in the *xy*-plane without (Fig. 4a) and with (Fig. 4b) FD do not show any appreciable distortion in the density image which can be corroborated in the 1D profile shown in Fig. 4c. The same analysis was performed for the *xz*-plane (see Fig. 4d–e). The *z*-velocity maps for flow conditions through the inner and the outer tube with the FD placed around the inner tube are shown in Fig. 5a and b, respectively. For both situations, a parabolic behavior is observed. A comparison between the results obtained with and without the FD (Fig. 5c and d) demonstrate that no distortions are observed due to the presence of the FD.

3.3. Intra-aneurismal flow measurements

Velocity maps along the *x*- and *z*-axes were measured at 1.5 ml/s flow rate in the vessel glass phantoms (see Fig. 6). A maximum velocity of approximately 180 mm/s could be observed along the long axis of both vessels. A negligible flow was observed inside the aneurysm for the straight vessel, whereas velocities of up to 50 mm/s were generated inside the aneurysm on the V-shaped vessel. If the flow rate is increased to 2.3 ml/s, the intra-aneurismal flow generated inside the aneurysm of the V-shaped vessel also increases. No appreciable change in the aneurysm was observed with increasing flow rate in the straight phantom geometry. The fact that for a curved vessel the flow towards the aneurysm neck renders a higher inflow upon different flow conditions (steady or pulsatile flow) than in a straight vessel geometry, has been previously reported for *in vitro* studies using PIV [1].

Fig. 7a) and b) shows the *y*- and *z*-velocity maps in the aneurysm sack for the V-shaped vessel, respectively. By combining both velocity maps, a velocity vector map is obtained (Fig. 7c), and a rotational vortex in the flow pattern with a maximum velocity of 200 mm/s can be observed inside the aneurysm. As mentioned before, FDs can redirect the flow in the vessel and can slow down the intra-aneurismal flow. The FD was inserted into the main vessel of the V-shaped phantom. In this case, the maximum velocity measured inside the aneurysm was 20 mm/s (Fig. 7d–f), while the mainstream flow through the vessel was not altered. The rotational vortex was greatly reduced (Fig. 7f).

A 3D structural image of the silicone phantom can be seen in blue at the left side of Fig. 8. The MRI image was obtained by acquiring the signal with a spin-echo sequence under steady flow conditions without the presence of the FD. The projection of the velocity

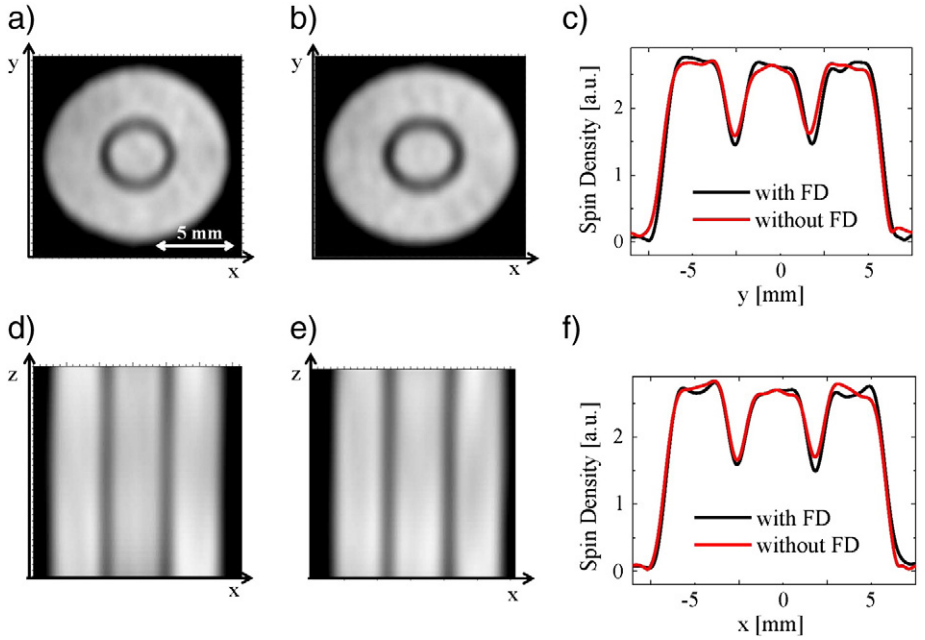

Fig. 4. Sensitivity of the MR images to the presence of the metallic FD: a) and b) *xy*-plane of a 3D image of the test sample without and with FD, respectively. The 3D images were acquired with a spatial resolution of 0.5 × 0.5 × 1 mm^3 averaging 4 scans. c) Comparison of a 1D density profile along the *y*-axis with and without the FD. d) and e) *xz*-plane of a 3D image with and without the FD, respectively. f) 1D density profiles along the *x*-axis measured with and without the FD.

measurements on the *zy*- and *yx*- planes are shown in Fig. 8a) and b) respectively. The measurements were carried out with and without the FD for a flow rate of 1.5 ml/s. The velocity distribution in the plane transverse to the main vessel input stream indicated in Fig. 8a — vector map — shows a rotational vortex (circular region in vector plot) with velocity amplitudes transverse of up to 80 mm/s. When the FD is inserted in the phantom, the velocities are reduced to values of approx. 20 mm/s. Noteworthy is that the *z*-velocity

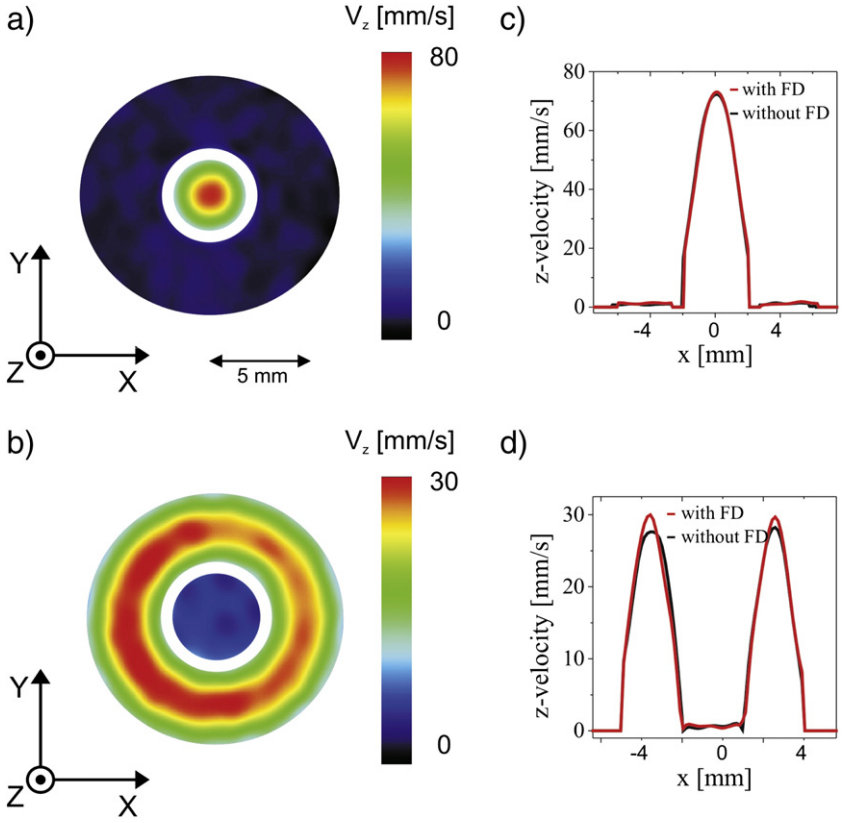

Fig. 5. Sensitivity of the flow measurements to the presence of the metallic FD: *z*-velocity map measured with the FD for the test-sample, where the fluid flows through a) the inner tube and b) the outer tube. c) and d) 1D-Cross sections of the *z*-velocity maps with and without the FD and taken under flow conditions through the inner tube and the outer tube, respectively. The Reynolds number was 100 and 40 for flow through the inner and outer tube, respectively.

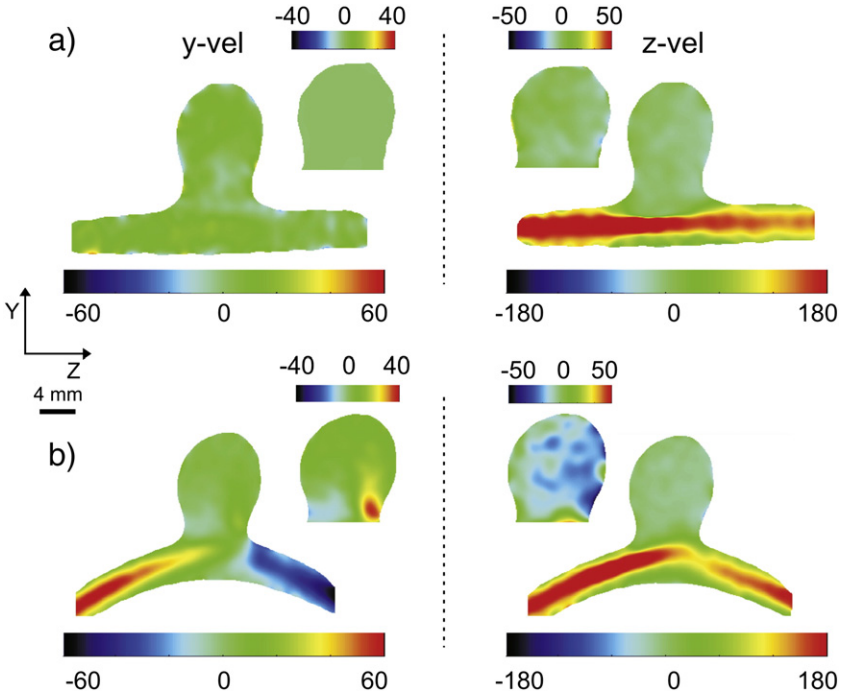

Fig. 6. Effect of the vessel geometry on the intra-aneurismal flow: *y*- and *z*-velocity maps in the a) straight vessel geometry and b) V-shaped vessel geometry. Using a flow rate of 1.5 ml/s, the Reynolds numbers were 250 in the vessel and 60 in the aneurysm. The spatial resolution was 0.9 × 0.6 × 0.8 mm^3, and after averaging 16 scans, the total experimental time for each map was 68 min.

component is reduced from 150 mm/s to 10–20 mm/s when the FD is introduced inside the aneurysm; this can be seen in the *xy*-plane (Fig. 8b z-velocity).

4. Discussion

The presented results demonstrate a satisfactory performance of the desktop MRI tomograph working at 0.2 T with a sensitive volume diameter of 40 mm to measure velocity. The accuracy of the system was determined using a test-sample which generates a known spatial velocity distribution. By using a spin echo pulse sequence, three velocity components were measured, detecting velocity amplitudes of up to 200 mm/s with an accuracy of 1% in an experimental time of about 15 min. In contrast to working at higher magnetic fields, one major advantage of using such a low magnetic field is that the presence of a metallic FD neither influences the amplitude nor the phase of the NMR signal.

The flow patterns measured for spherical aneurysms connected to straight and V-shaped vessel (glass phantoms) agree with the ones reported in the literature, where shear-driven flow, with very low velocities inside the aneurysm, is reported for a straight vessel. However, inertia-driven flow is present in a curved vessel geometry, with the presence of a strong rotational vortex inside the aneurysm [1]. For the V-shaped vessel, the flow patterns in the presence of the FD were measured. Hereby a decrease of one order of magnitude in

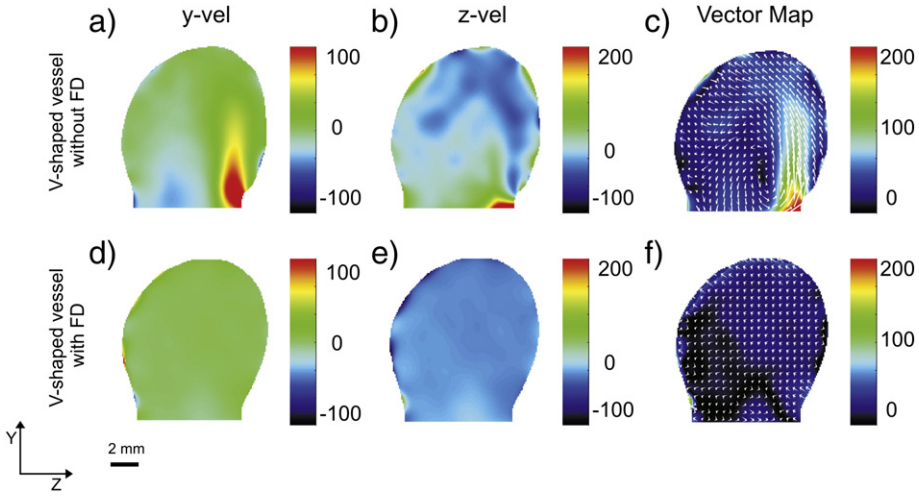

Fig. 7. FD effect on the intra-aneurismal flow in the V-shaped glass vessel aneurysm. a) Velocity maps in *y*- and b) *z*-axes measured without the FD for a flow rate of 2.3 ml/s. c) Velocity vector field in the *yz*-plane. d) Velocity map in *y*- and e) *z*-axes and f) velocity vector field measured with FD. For this flow condition the Reynolds number was 185. Each map was acquired with a spatial resolution of 0.9 × 0.6 × 0.8 mm^3 and 16 scans, resulting in a total experimental time of 68 min.

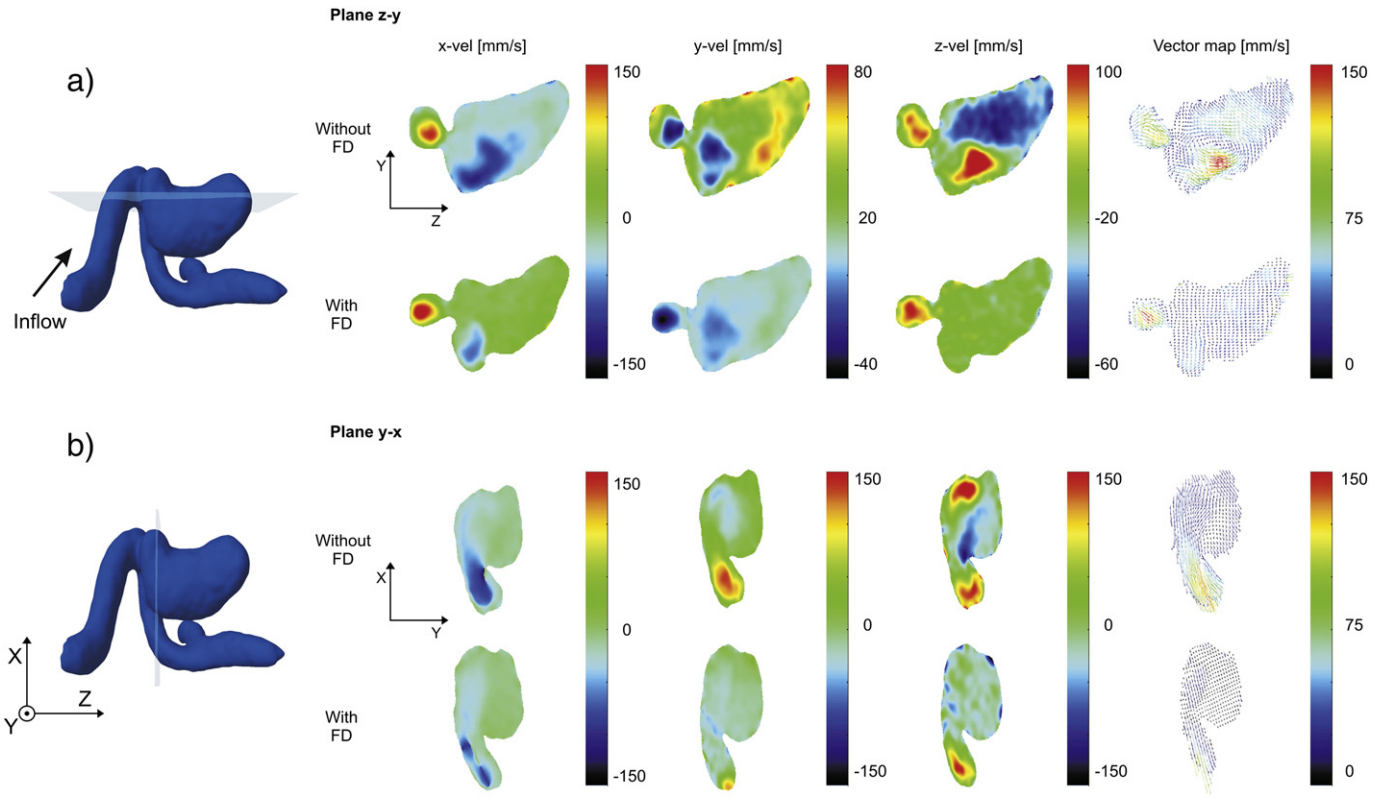

Fig. 8. Intra-aneurismal flow measurements in a silicone model of an aneurysm mapped from a patient. a) 3D MRI structure showing the *zy*-plane where the three components of the velocity and the velocity vector map are plotted with and without the FD. b) The same as a) but shown on an *xy*-plane. The Reynolds number was 370. Each map was acquired with a spatial resolution of 0.6 × 0.6 × 0.8 mm^3 and 4 scans resulting in a total experimental time of 77 min.

the velocities inside the glass aneurysm was determined, while the mainstream velocity was unaffected by the presence of the metallic mesh.

The velocity map inside a model silicone aneurysm with a geometry mapped from a live patient was characterized with and without the presence of an FD. In the absence of the FD, the flow pattern is quite complex. A 3D structural image was acquired as a reference, and all velocity components were displayed in two representative planes in the aneurismal sac. Measurements were carried out with a constant flow rate of 1.5 ml/s, giving rise to a mainstream velocity in the vessels of 140 mm/s, as observed in the *x*-velocity in Fig. 8a. Here it can be observed that the presence of the FD does not change the magnitude of the incoming velocity of the glycerin/water mixture in the main vessel. Inside the aneurismal sac, a rotational vortex is observed mainly in the *yz*-plane with velocities of up to 80 mm/s, which is mostly in the *z*-component. The principal inflow into the aneurysm can be identified in the higher region of the image corresponding to the *z*-component of the *yx*-plane (Fig. 8b). Upon the positioning of the FD, this inflow is clearly suppressed, and the rotational vortex is greatly reduced, with velocities reaching a maximum value of 20 mm/s.

It has to be taken into account that in order to show the performance of the low-field system in this initial step, simplified conditions such as constant flow and spin-echo acquisition were implemented. In order to obtain an evaluation under more realistic conditions, the use of pulsatile flow instead of steady flow needs to be considered. Pulsatile flow can be implemented by synchronizing the acquisition of the MRI signal with the pump pulse period. When this strategy is combined with the spin-echo pulse sequence, the repetition time t_R between acquisitions should match the pulse period, which is typically of about 1 s [1]. Assuming a regular behavior of the flow in the aneurysm system (neither amplitude nor frequency changes), each line of the *k*-space is sampled always at the same phase of the cardiac cycle (diastolic flow, mid or peak systolic flow), i.e., every 1 s. This approach would allow one to obtain flow maps at well defined phases of the cardiac cycle, since the acquisition of one *k*-space line lasts about 500 μs, which is three orders of magnitude shorter than the cardiac cycle (1 s). However, the procedure would still be time-consuming.

A significant reduction in the experimental time is achieved by using fast imaging pulse sequences based on multi-echo acquisition. Due to the short T^*_2 of the actual system, the use of a multiple gradient-echo scheme would not be optimal. Nevertheless, there are commercially available systems in which this could be implemented. We have previously shown the performance of the RARE or turbo spin-echo sequence implemented in this sensor [19]. The combination of this last MR imaging scheme with suitable velocity encoding [24] would help to reduce the acquisition time for velocity maps in routine applications. The total acquisition time of the image would be 150 ms with an echo time of about 5 ms and by considering a spatial resolution that ranges from 0.5 to 1 mm, which leads to ~ 30 steps (echoes) along the phase direction of the *k*-space for a FoV from 15 mm to 30 mm. In this way, a substantial reduction in experimental time would be obtained. Yet the flow map would correspond to an average of about 1/6 (150/1000) of the cardiac cycle.

Most of the *in vitro* experiments studying the effect of stents on intra-aneurismal flow have used optical techniques such as LDA and PIV which present higher spatial resolutions than MRI. In particular, for PIV the range of velocity magnitudes measured in aneurysm systems of similar size as the ones reported here coincides with the one obtained in the present work [1,25–27]. However, these

techniques require optically transparent fluid and the inclusion of external particles used as tracers. The use of high-field MRI to evaluate in-stent stenosis have reported velocity errors of about 0.1% [11]. This error was determined using an analysis based on SNR of one MR image which does not consider the reproducibility of the experiment. By applying such an analysis to our measurements where an SNR of about 100 was obtained (see Fig. 4d) and e)), we would have an error of the velocity determination of 0.3%. The difference of this value with the three times larger error calculated by statistical error analysis, shown in Fig. 3, can be attributed to instabilities of the flow setup.

Future implementation of pulsatile flow conditions and rapid velocity imaging sequences will render this type of setup optimal to establish the correlation between clot formation, via T_1 and/or T_2 mapping, with the intra-aneurismal flow reduction induced by the FD. In combination with clinical MRI systems, this scenario will be very promising in order to decide the best FD parameters to be used for a particular patient.

Finally, it is noteworthy that the use of a low-field system for flow determination is not restricted to the particular medical application described here, but also for process and quality control, or velocimetry measurements in chemical engineering systems such as micromixers or microreactors. Moreover, because of the versatility of a desktop MRI system, it can be adapted to different experimental scenarios. For instance, the magnet can be easily set in a vertical position and imaging of velocity distributions such as those produced in Couette Cells for the mixing of fluids, or the combination with rheology setups [28] can be readily applied.

5. Conclusions

Velocity-MRI can be successfully carried out in compact tomographs based on arrays of permanent magnets. Velocity magnitudes of up to 200 mm/s with a precision of 1% inside aneurysm phantoms made from glass and silicone were measured. It was observed that the presence of metallic implants did not introduce artifacts in the amplitude nor in the phase of the NMR signal. Significant changes in flow pattern distributions and velocity magnitudes were observed after insertion of a flow diverter (FD).

The spatial resolution and precision of the velocity mapping technique reported in this work prove to be suitable for characterizing the influence of an FD on the intra-aneurismal flow distribution for the proposed *in-vitro* approach. As the degree and the time of occlusion depend on several physiological and FD parameters, searching for the FD that leads to the optimum clot formation speed for a given patient is very time-consuming and, thus, impracticable in conventional clinical scanners. The promising performance of the sensor presented here is an impetus for designing and selecting tailor-made FDs in the future for individual patients in order to avert aneurysm rupture.

Acknowledgements

We wish to thank BMBF-Germany and MinCyT-Argentina for the cooperation program that made this work possible. DFG (Gerätezentrum Pro2NMR), CONICET, FoNCyT and SeCyT-UNC are kindly acknowledged for providing financial support. We would also like to acknowledge Dr. med Vitor Mendes Pereira from the Institute of Interventional Neuroradiology Unit, University Hospital of Geneva for providing the silicone phantom.

References

[1] Augsburger L, Farhat M, Reymond P, Fonck E, Kulcsar Z, Stergiopulos N, et al. Effect of flow diverter porosity on intraaneurysmal blood flow. Klin Neuroradiol 2009;19(3):204–14.
[2] Pereira VM, Bonnefous O, Ouared R, Brina O, Stawiaski J, Aerts H, et al. A DSA-based method using contrast-motion estimation for the assessment of the intra-aneurysmal flow changes induced by flow-diverter stents. AJNR Am J Neuroradiol 2013;34(4):808–15.
[3] Shapiro M, Babb J, Becske T, Nelson PK. Safety and efficacy of ad- junctive balloon remodeling during endovascular treatment of intracranial aneurysms: a literature review. AJNR Am J Neuroradiol 2008;29(9):1777–81.
[4] Kallmes D, Hong Ding Y, Dai D, Kadirvel R, Lewis DA, Cloft HJ. A new endoluminal, flow-disrupting device for treatment of saccular aneurysms. Stroke 2007;38:2346–52.
[5] Bing F, Darsaut TE, Salazkin I, Makoyeva A, Gevry G, Raymond J. Stents and flow diverters in the treatment of aneurysms: device deformation in vivo may alter porosity and impact efficacy. Neuroradiology 2013;55(1):85–92.
[6] Kulcsár Z, Houdart E, Bonafé A, Parker G, Millar J, Goddard AJP, et al. Intra-aneurysmal thrombosis as a possible cause of delayed aneurysm rupture after flow-diversion treatment. AJNR Am J Neuroradiol 2011;32(1):20–5.
[7] Hampton T, Walsh D, Tolias C, Fiorella D. Mural destabilization after aneurysm treatment with a flow-diverting device: a report of two cases. J Neurointerv Surg 2011;3(2):167–71.
[8] Harlow FH. Fluid dynamics in group T-3 Los Alamos National Laboratory. J Comput Phys 2004;195:414–33.
[9] Weichert F, Walczak L, Fisseler D, Opfermann T, Razzaq M, Münster R, et al. Simulation of intra-aneurysmal blood flow by different numerical methods. Comput Math Methods Med 2013;2013:1–10 527654.
[10] Biglino G, Verschueren P, Zegels R, Taylor AM, Schievano S. Rapid prototyping compliant arterial phantoms for in-vitro studies and device testing. J Cardiovasc Magn Reson 2013;15(2):1–7.
[11] Holton AD, et al. Evaluation of in-stent stenosis by magnetic resonance phase-velocity mapping in nickel-titanium stents. J Magn Reson Imaging 2005;22(2):248–57.
[12] Walsh EG, Holton AD, Brott BC, Venugopalan R, Anayiotos AS. Magnetic resonance phase velocity mapping through NiTi stents in a flow phantom model. J Magn Reson Imaging 2005;21(1):59–65.
[13] Dorn F, Niedermeyer F, Balasse A, Liepsch D, Liebig T. The effect of stents on intra -aneurysmal hemodynamics: in vitro evaluation of a pulsatile sidewall aneurysm using laser Doppler anemometry. Neuroradiology 2011;53(4):267–72.
[14] Cebral JR, Mut F, Raschi M, Scrivano E, Ceratto R, Lylyk P, et al. Aneurysm rupture following treatment with flow-diverting stents: computational hemodynamics analysis of treatment. AJNR Am J Neuroradiol 2011;32(1):27–33.
[15] Shobayashi Y, Tateshima S, Kakizaki R, Sudo R, Tanishita K, Vinuela F. Intra-aneurysmal hemodynamic alterations by a self-expandable intracranial stent and flow diversion stent: high intra-aneurysmal pressure remains regardless of flow velocity reduction. J Neurointerv Surg 2013;5(3):iii38–42.
[16] Liou TM, Li YC. Effects of stent porosity on hemodynamics in a sidewall aneurysm model. J Biomech 2008;41(6):1174–83.
[17] Mücke T, Ritschl LM, Balasso A, Wolff KD, Liepsch D. Flow analyses of microvascular bifurcation using laser Doppler anemometry. J Reconstr Microsurg 2013;29(6):399–406.
[18] Hoskins PR. Simulation and validation of arterial ultrasound imaging and blood flow. Ultrasound Med Biol 2008;34(5):693–717.
[19] Danieli E, Mauler J, Perlo J, Blümich B, Casanova F. Mobile sensor for high resolution NMR spectroscopy and imaging. J Magn Reson 2009;198(1):80–7.
[20] Moran PR. A flow velocity zeugmatographic interface for NMR imaging in humans. Magn Reson Imaging 1982;1(4):197–203.
[21] Hahn EL. Detection of sea-water motion by nuclear precession. J Geophys Res 1960;65(2):776–7.
[22] Wang Y, Truong TN, Yen Cecil, Bilecen D, Watts R, Trost DW, et al. Quantitative evaluation of susceptibility and shielding effects of nitinol, platinum, cobalt-alloy, and stainless steel stents. Magn Reson Med 2003;49(5):972–6.
[23] Karacozoff AM, Shellock FG, Wakhloo AK. A next-generation, flow-diverting implant used to treat brain aneurysms: in vitro evaluation of magnetic field interactions, heating and artifacts at 3-T. Magn Reson Imaging 2013;31:145–9.
[24] Amar A, Blümich B, Casanova F. Rapid multiphase flow dynamics mapped by single-shot MRI velocimetry. Chemphyschem 2010;11:2630–8.
[25] Lieber BB, Livescu V, Hopkins LN, Wakhloo AK. Particle image velocimetry assessment of stent design influence on intraaneurysmal flow. Ann Biomed Eng 2002;30(6):768–77.
[26] Ford MD, Nikolov HN, Milner JS, Lownie SP, Demont EM, Kalata W, et al. PIV-measured versus CFD-predicted flow dynamics in anatomically realistic cerebral aneurysm models. J Biomech Eng 2008;130(2):1–9 021015.
[27] Trager AL, Sadasivan C, Seong J, Lieber BB. Correlation between angiographic and particle image velocimetry quantifications of flow diverters in an in vitro model of elastase-induced rabbit aneurysms. J Biomech Eng 2009;131(3):1–3 034506.
[28] Callaghan PT. Rheo-NMR: nuclear magnetic resonance and the rheology of complex fluids. Rep Prog Phys 1999;62:599–668.